Pattern Recognition 44 (2011) 187–195

Contents lists available at ScienceDirect

Pattern Recognition

journal homepage: www.elsevier.com/locate/pr

Quaternion Fourier–Mellin moments for color images

Li-Qiang Guo [a,b,*], Ming Zhu [a]

[a] Changchun Institute of Optics, Fine Mechanics and Physics, Chinese Academy of Science, Changchun 130033, China
[b] Graduate school of Chinese Academy of Science, Chinese Academy of Science, Beijing 100039, China

ARTICLE INFO

Article history:
Received 31 December 2009
Received in revised form
4 August 2010
Accepted 10 August 2010

Keywords:
Quaternion
Quaternion Fourier–Mellin moments
Moment invariant
Color image registration

ABSTRACT

The quaternion Fourier–Mellin moments for describing color images are introduced, which can be seen as the generalization of traditional Fourier–Mellin moments for gray-level images. Then, the quaternion Fourier–Mellin moment invariants are derived, which could be a useful tool in color object recognition tasks that require the similarity invariance. In addition, the problem of color image registration using quaternion Fourier–Mellin moments is discussed. The registration method can match color images differing in rotation and scaling. The advantage of our method is that it can process color image directly, without losing color information. Experimental results validate the effectiveness of the method we proposed.

1. Introduction

A main issue in pattern recognition is to find the invariant with respect to geometric transform, such as: rotation, scaling and translation. Moment invariants can deal with such geometric transform. The pioneering work of moment invariants was done by Hu [1] as image recognition features which had the property of being invariant under such geometric transform. Since then, various types of moment functions are constructed, such as complex moment [2], Legendre and Zernike moments [3], pseudo-Zernike moments [4], Chebyshev–Fourier moments [5], Racah moments [6], dual Hahn moments [7], and so on. Besides, some excellent works have made outstanding contribution to the theory of moment invariants [8–13].

However, we are concerned of the Fourier–Mellin moments, which were first introduced in optical research community [14,15]. Shortly, Fourier–Mellin descriptor was presented in [16–18] for image processing. In [19], orthogonal Fourier–Mellin moments were introduced based on a set of radial polynomials. There is also a group of excellent works associated with Fourier–Mellin moments [20–23]. But, Fourier–Mellin moments used in the papers mentioned above are dealt with gray-level images, none of them processing color images. In this study, we generalized the traditional Fourier–Mellin moments from real and complex numbers to quaternion algebra. Quaternion Fourier–Mellin moments (QFMMs) for describing color images were proposed.

Registration is a fundamental task in image processing to match two or more images of the same scene taken at different times, from different viewpoints or by different sensors. Traditional image registration methods are dealt with gray-level images, such as correlation methods [24,25], feature-based methods [26–30], methods that use the frequency domain [31–33], and so on. We study the application of QFMMs into color image registration and propose an algorithm for the alignment of color images differing in rotation and scaling.

The paper is organized as follows. First, in Section 2 we give a brief introduction of quaternion and quaternion Fourier transform (QFT). Then, in Section 3 we introduce the quaternion Fourier–Mellin moments and its invariants for rotation, scaling and translation of color images. In addition, we discuss the method of color image registration using QFMMs in Section 4. Moreover, experimental results are described in Section 5. Finally, conclusions are made in Section 6.

2. Preliminaries

2.1. Quaternion

The quaternion, which is a type of hypercomplex number, was formally introduced by Hamilton in 1843 [35]. It is a generalization of complex number. We know that a complex number has two components: the real part and imaginary part. However, the quaternion has four parts, that are, one real part and three

* Corresponding author at: Changchun Institute of Optics, Fine Mechanics and Physics, Chinese Academy of Science, Yingkou Road No. 88, Economic and Technology District, Changchun, Jilin Province, 130033, China.
Tel.: +86 043186176557; fax: +86 043185893419.
E-mail addresses: math_circuit@qq.com (L.-Q. Guo), zhu_mingca@163.com (M. Zhu).

0031-3203/$ - see front matter © 2010 Elsevier Ltd. All rights reserved.
doi:10.1016/j.patcog.2010.08.017

imaginary parts. For a quaternion q, which can be written in a hypercomplex form as follows: $q=q_r+q_ii+q_jj+q_kk$, where q_r, q_i, q_j, q_k are real numbers and i,j,k are complex operators obeying the following rules:

$$i^2=j^2=k^2=-1, \quad ij=-ji=k, \quad jk=-kj=i, \quad ki=-ik=j \tag{1}$$

From Eq. (1), we find that the multiplication rule of quaternions is not commutative.

Sometimes, a quaternion is considered as the combination of a scalar part and a vector part: $q=S(q)+V(q)$, where $S(q)=q_r$, $V(q)=q_ii+q_jj+q_kk$. If a quaternion q has a zero scalar part ($q_r=0$), then q is called pure quaternion, and if q has a unit norm ($\|q\|=1$), then q is called unit pure quaternion.

The conjugate of a quaternion q is: $\overline{q}=q_r-q_ii-q_jj-q_kk$. For any two quaternions p and q, then: $\overline{p\cdot q}=\overline{q}\cdot\overline{p}$.

The norm of q is: $\|q\|=\sqrt{q\cdot\overline{q}}=\sqrt{q_r^2+q_i^2+q_j^2+q_k^2}$.

In [34], Sangwine proposed to encode the three channel components of an RGB image on the three imaginary parts of a pure quaternion. In other words, a pixel at image coordinate (m,n) in an RGB image can be represented as

$$f(m,n)=f_R(m,n)i+f_G(m,n)j+f_B(m,n)k \tag{2}$$

where $f_R(m,n)$, $f_G(m,n)$ and $f_B(m,n)$ are the red, green and blue components of the pixel, respectively.

Euler's formula holds for quaternions, that is, $e^{\mu\phi}=\cos(\phi)+\mu\cdot\sin(\phi)$. We also have: $\|e^{\mu\phi}\|=1$.

The quaternion q can be represented in polar form: $q=\|q\|e^{\mu\phi}$, where μ and ϕ are called eigenaxis and eigenangle, respectively. μ and ϕ are computed by: $\mu=V(q)/\|V(q)\|$, $\phi=\arctan\|V(q)\|/S(q)$. For a more complete discussion about the properties of quaternion can be found in Ref. [35].

2.2. Quaternion Fourier transform

As the generalization of traditional Fourier transform, quaternion Fourier transform was first defined by Ell to process quaternion signals [36]. Later, some constructive works related to quaternion Fourier transform and its application in color image processing are presented in [37–42]. From last subsection, due to the noncommutative property of quaternion multiplication, there are three different definitions of two-dimensional quaternion Fourier transform as follows:

$$F^{(l)}(\omega,v)=\int_{-\infty}^{\infty}\int_{-\infty}^{\infty}e^{-\mu_1(\omega x+vy)}f(x,y)\,dx\,dy \tag{3}$$

$$F^{(r)}(\omega,v)=\int_{-\infty}^{\infty}\int_{-\infty}^{\infty}f(x,y)e^{-\mu_1(\omega x+vy)}\,dx\,dy \tag{4}$$

$$F^{(t)}(\omega,v)=\int_{-\infty}^{\infty}\int_{-\infty}^{\infty}e^{-\mu_1\omega x}f(x,y)e^{-\mu_2 vy}\,dx\,dy \tag{5}$$

where μ_1 and μ_2 are two unit pure quaternions that are orthogonal to each other. The three QFTs are defined by placing the integral kernels $e^{-\mu_1\omega x}$ and $e^{-\mu_2 vy}$ on the left side, right side and one on two sides of a quaternion signal $f(x,y)$. Therefore, $F^{(l)}(\omega,v)$, $F^{(r)}(\omega,v)$ and $F^{(t)}(\omega,v)$ are called left-side, right-side and two-side QFT, respectively.

3. Quaternion Fourier–Mellin moment invariants

3.1. Quaternion Fourier–Mellin moments (QFMMs)

Let $f(r,\theta)$ be the gray-level image in polar coordinates, the traditional Fourier–Mellin moments of $f(r,\theta)$ were defined as follows:

$$M_{s,l}=\int_{r=0}^{\infty}\int_{\theta=0}^{2\pi}r^{s-1}e^{-il\theta}f(r,\theta)\,d\theta\,dr \tag{6}$$

Enlightened by the definition of Fourier–Mellin moments, we combined the one-dimensional quaternion Fourier transform with Mellin transform to define the quaternion Fourier–Mellin moments.

Definition 1. Let $f(r,\theta)=f_R(r,\theta)i+f_G(r,\theta)j+f_B(r,\theta)k$ represents an *RGB* image defined in polar coordinates, the $(m+n)$th order left-side quaternion Fourier–Mellin moments of $f(r,\theta)$ are given by

$$QFM_l[f(r,\theta);\mu](m,n)=\int_{r=0}^{\infty}\int_{\theta=0}^{2\pi}r^{m-1}e^{-\mu n\theta}f(r,\theta)\,d\theta\,dr \tag{7}$$

where m, n are positive integers and μ is any unit pure quaternion, for example: $\mu=i$, $\mu=j$, $\mu=k$, $\mu=(\sqrt{2}/2)i+(\sqrt{2}/2)k$, $\mu=(\sqrt{3}/3)i+(\sqrt{3}/3)j+(\sqrt{3}/3)k$, etc.

Similar as the definition of quaternion Fourier transform, the right-side quaternion Fourier–Mellin moments are defined by placing the integral kernel $e^{-\mu n\theta}$ on the right side of $f(r,\theta)$:

$$QFM_r[f(r,\theta);\mu](m,n)=\int_{r=0}^{\infty}\int_{\theta=0}^{2\pi}r^{m-1}f(r,\theta)e^{-\mu n\theta}\,d\theta\,dr \tag{8}$$

In Section 2.1, we have known that for any two quaternions p and q, then $\overline{p\cdot q}=\overline{q}\cdot\overline{p}$. We will use this anti-involution property of quaternion conjugation to establish the relationship between left-side and right-side QFMMs for the same color image $f(r,\theta)$:

$$\begin{aligned}QFM_r[f(r,\theta);\mu](m,n)&=\overline{\int_{r=0}^{\infty}\int_{\theta=0}^{2\pi}r^{m-1}f(r,\theta)e^{-\mu n\theta}\,d\theta\,dr}\\&=\overline{\int_{r=0}^{\infty}\int_{\theta=0}^{2\pi}r^{m-1}\overline{e^{-\mu n\theta}}\cdot\overline{f(r,\theta)}\,d\theta\,dr}\\&=\overline{\int_{r=0}^{\infty}\int_{\theta=0}^{2\pi}r^{m-1}e^{\mu n\theta}\cdot\overline{f(r,\theta)}\,d\theta\,dr}\\&=\overline{QFM_l[\overline{f(r,\theta)};-\mu](m,n)}\end{aligned} \tag{9}$$

Eq. (9) indicates that we can compute right-side QFMMs through left-side QFMMs. From Eq. (9) and experimental results in Section 5.4, we can conclude that left-side and right-side QFMMs are equivalent to describe similarity transforms of color image. In this paper, the quaternion Fourier–Mellin moments refers to left-side QFMMs and denoted as "$Q_{m,n}$" for abbreviation.

The similarity] transform of a color image consists of rotation, translation and uniform scale transform. Suppose $f(x',y')$ is the transformed replica of original image $f(x,y)$. We can use a matrix equation to represent similarity transform as follows:

$$\begin{pmatrix}x'\\y'\end{pmatrix}=a\begin{pmatrix}\cos\varphi & -\sin\varphi\\ \sin\varphi & \cos\varphi\end{pmatrix}\begin{pmatrix}x\\y\end{pmatrix}+\begin{pmatrix}\Delta x\\ \Delta y\end{pmatrix} \tag{10}$$

where a is the scale factor with $a>0$, φ is the rotation angle, Δx and Δy are the translation offset along x- and y-axes, respectively.

3.2. Rotation invariance

Let $f(r,\theta+\varphi)$ denotes the rotation change of a color image $f(r,\theta)$ by the angle φ, then quaternion Fourier–Mellin moments of $f(r,\theta+\varphi)$ and $f(r,\theta)$ have the following relations:

$$\begin{aligned}Q'_{m,n}&=\int_{r=0}^{\infty}\int_{\theta=0}^{2\pi}r^{m-1}e^{-\mu n\theta}f(r,\theta+\varphi)\,d\theta\,dr\\&=e^{\mu n\varphi}\int_{r=0}^{\infty}\int_{\theta=0}^{2\pi}r^{m-1}e^{-\mu n\theta}f(r,\theta)\,d\theta\,dr\\&=e^{\mu n\varphi}Q_{m,n}\end{aligned} \tag{11}$$

where $Q'_{m,n}$ and $Q_{m,n}$ are the QFMMs of $f(r,\theta+\varphi)$ and $f(r,\theta)$, respectively.

According to Eq. (11), we know that a rotation of the color image by an angle φ induces a phase shift $e^{\mu n\varphi}$ of the $Q_{m,n}$. Taking the norm on both sides of Eq. (11), we have

$$\|Q'_{m,n}\| = \|e^{\mu n\varphi}Q_{m,n}\| = \|e^{\mu n\varphi}\| \cdot \|Q_{m,n}\| = \|Q_{m,n}\| \tag{12}$$

So, the rotation invariance can be achieved by taking the norm of the color images' QFMMs. In other words, $\Phi_{m,n} = \|Q_{m,n}\|$ are invariant with respect to rotation transform.

3.3. Scale invariance

Suppose $f(ar,\theta)$ be the color image expanded by the scale factor a, then the following equation holds:

$$\begin{aligned} Q'_{m,n} &= \int_{r=0}^{\infty}\int_{\theta=0}^{2\pi} r^{m-1}e^{-\mu n\theta}f(ar,\theta)\,d\theta\,dr \\ &= \int_{r=0}^{\infty}\int_{\theta=0}^{2\pi} \left(\frac{r}{a}\right)^{m-1}e^{-\mu n\theta}f(r,\theta)\frac{1}{a}\,d\theta\,dr \\ &= a^{-m}\int_{r=0}^{\infty}\int_{\theta=0}^{2\pi} r^{m-1}e^{-\mu n\theta}f(r,\theta)\,d\theta\,dr \\ &= a^{-m}Q_{m,n} \end{aligned} \tag{13}$$

where $Q'_{m,n}$ and $Q_{m,n}$ are the QFMMs of $f(ar,\theta)$ and $f(r,\theta)$, respectively.

If $n=0$ in Eq. (13), we have: $Q'_{m,0} = a^{-m}Q_{m,0}$. The scale invariants can be constructed as follows:

$$\Phi_{m,n} = \frac{Q'_{m,n}}{Q'_{m,0}} = \frac{a^{-m}Q_{m,n}}{a^{-m}Q_{m,0}} = \frac{Q_{m,n}}{Q_{m,0}} \tag{14}$$

The value of scale invariant is a quaternion. For any two different quaternions, we cannot compare them directly, but we can compare the norm of the invariants of different scaling color images.

We can construct rotation and scale invariants as follows:

$$\Phi_{m,n} = \left\|\frac{Q_{m,n}}{Q_{m,0}}\right\| \tag{15}$$

Analogously, $\Phi_{m,n} = \|Q_{m,n}/(Q_{2,0})^{m/2}\|$ are also invariant under rotation and scale transforms.

3.4. Translation invariance

Translation invariance is achieved by putting the origin of coordinates at the color image centroid. First, we give the definition of the centroid of color image in Cartesian coordinates:

Definition 2. Let $f(x,y)$ be a color image, then the centroids of x- and y-coordinate, $\overline{x}$ and $\overline{y}$, respectively, are defined as follows:

$$\overline{x} = \frac{\sum_{x=1}^{M}\sum_{y=1}^{N} x\|f(x,y)\|}{\sum_{x=1}^{M}\sum_{y=1}^{N}\|f(x,y)\|}, \quad \overline{y} = \frac{\sum_{x=1}^{M}\sum_{y=1}^{N} y\|f(x,y)\|}{\sum_{x=1}^{M}\sum_{y=1}^{N}\|f(x,y)\|} \tag{16}$$

Let $f(x,y)$ and $f(x',y')$ denote the color image and its translated replica, respectively, where $x' = x+\Delta x$, $y' = y+\Delta y$ and $f(x,y) = f(x',y')$, then

$$x'-\overline{x'} = x+\Delta x-\frac{\sum_{x=1}^{M}\sum_{y=1}^{N}(x+\Delta x)\|f(x,y)\|}{\sum_{x=1}^{M}\sum_{y=1}^{N}\|f(x,y)\|} = x+\Delta x-\overline{x}-\Delta x = x-\overline{x} \tag{17}$$

Similarly, we have: $y'-\overline{y'} = y-\overline{y}$. Therefore, if we put the origin of coordinates at the color image centroid, the rotation and scale invariants constructed in the last subsection also have the property of being invariant under translation transform.

3.5. Numerical computation of QFMMs

The discrete form of QFMMs are given by

$$\begin{aligned} Q_{m,n} &= \sum_{r=0}^{r_{max}}\sum_{\theta=0}^{2\pi} r^{m-1}e^{-\mu n\theta}f(r,\theta)\Delta\theta\Delta r \\ &= \sum_{r=0}^{r_{max}} r^{m-1}\left[\sum_{\theta=0}^{2\pi} e^{-\mu n\theta}f(r,\theta)\Delta\theta\right]\Delta r \end{aligned} \tag{18}$$

The expression in square brackets of Eq. (18) can be seen as a discrete form of one-dimensional QFT with respect to variable θ, we can use the "*qfft*" function in Quaternion Toolbox for Matlab to fast computation of that part [43].

In the computation of QFMMs of a color image $f(x,y)$, we should first put the origin of Cartesian coordinates at the color image centroid, then change the color image from Cartesian coordinates to polar coordinates. The following step is to compute the QFMMs using Eq. (18). The detailed calculation steps are as follows:

Step 1: Calculate the centroid of color image $f(x,y)$ use Eq. (16) and put the origin of coordinates at the centroid.

Step 2: Calculate the "r_{max}", "Δr" and "$\Delta\theta$" using the following equations:

$$r_{max} = \max\{\sqrt{(x-\overline{x})^2+(y-\overline{y})^2}|x = 1,2,\ldots,M;\ y = 1,2,\ldots,N\},$$
$$\Delta r = \frac{r_{max}}{nrad-1}, \quad \Delta\theta = \frac{2\pi}{ntheta}$$

where the image size is $M\times N$ pixels, "nrad" and "ntheta" are the number of radius and angle value in polar coordinates, respectively.

Step 3: Change the color image from Cartesian coordinates to polar coordinates, we get $f(r,\theta)$.

Step 4: Calculate the QFMMs of $f(r,\theta)$ using Eq. (18).

4. Color image registration

This section presents a method of color image registration based on QFMM for computing transformation parameters from two images that differ by rotation and scale changes.

Let $f(ar,\theta+\varphi)$ be the color image expanded by the factor a and rotated by the angle φ, then quaternion Fourier–Mellin moments of $f(ar,\theta+\varphi)$ and $f(r,\theta)$ have the following relations:

$$\begin{aligned} Q'_{m,n} &= \int_{r=0}^{\infty}\int_{\theta=0}^{2\pi} r^{m-1}e^{-\mu n\theta}f(ar,\theta+\varphi)\,d\theta\,dr \\ &= a^{-m}e^{\mu n\varphi}\int_{r=0}^{\infty}\int_{\theta=0}^{2\pi} r^{m-1}e^{-\mu n\theta}f(r,\theta)\,d\theta\,dr \\ &= a^{-m}e^{\mu n\varphi}Q_{m,n} \end{aligned} \tag{19}$$

Let $m=1$ and $n=1$, then we can use Eq. (19) to derive the rotation angle φ, that is,

$$\Phi = \frac{Q'_{1,1}}{Q_{1,1}} = \frac{a^{-1}e^{\mu\varphi}Q_{1,1}}{Q_{1,1}} = a^{-1}e^{\mu\varphi} = a^{-1}(\cos(\varphi)+\mu\cdot\sin(\varphi)) \tag{20}$$

we can get the rotation angle φ through computing the real or imaginary part of Φ using inverse trigonometric function.

Using Eq. (19), we can also get the scale factor a as follows:

$$a = \left\|\frac{Q_{1,1}}{Q'_{1,1}}\right\| \tag{21}$$

Some important implementation details are presented here to estimate the parameters of rotation and scale transformations:

(1) The origin of polar coordinates is in the color image center $(M/2,N/2)$.
(2) When we estimate the rotation angle, the "r_{max}" in Eq. (18) is computed as follows:

$$r_{max}=\max\left\{\sqrt{\left(x-\frac{M}{2}\right)^2+\left(y-\frac{N}{2}\right)^2}\,|x=1,2,\ldots,M;\ y=1,2,\ldots,N\right\} \tag{22}$$

(3) When we estimate the scale factor, the computation of "r_{max}" is given by

$$r_{max}=\min\left\{\frac{M}{2}-1,\frac{N}{2}-1\right\} \tag{23}$$

Once the rotation and scaling parameters are determined, we can match the two color images using the inverse transforms and interpolation algorithms. The experimental results are shown in the next section.

5. Experiments

This section is intended to validate the effectiveness of the proposed QFMM invariants under similarity transform for color images. We also present the experimental results for registration performance of the proposed algorithm with traditional FFT-based method. In the following subsections, we specify the unit pure quaternion $\mu=\sqrt{2}/2\cdot i+\sqrt{2}/2\cdot k$ to compute QFMMs, and compute lower order QFMM invariants using Eq. (15). The program was implemented in Matlab 7.5 on a PC DuoCore 2.2 GHz, 4 G RAM.

5.1. Experiment on rotation invariance

We first evaluate the performance of the QFMM invariants under rotation transform. The original color image we used is selected from the Coil-100 image database of Columbia University [44]. The original and rotated images are shown in Fig. 1, where car_r0 is the original image, from car_r1 to car_r7 are the rotated version of original one. All these images are 128×128 pixels. The experimental results can be found in Table 1. Each column in Table 1 is the values of same moment invariant for different images; each row is the values of different moment invariants for the same image. The bottom row is the standard deviation of each column data to indicate the stability of the moment invariants.

As one can see from Table 1, the QFMM invariants remain almost unchanged under different rotation changes and most of the standard deviations are less than 0.02. Therefore, the QFMM invariants derived in this paper could be a useful tool in color object recognition tasks that require the rotation invariance.

5.2. Experiment on scale invariance

The goal of this subsection is to evaluate the performance of the QFMM invariants under scale transform. The original color image is car_s0, others are the scaled version of original one.

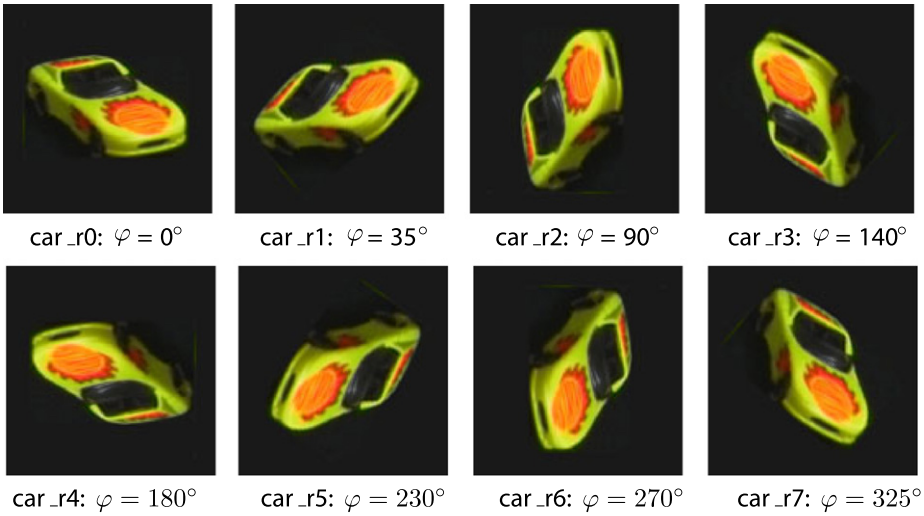

Fig. 1. The original color image and its rotated version for rotation invariance tests.

Table 1
QFMM invariants of the same color image under rotation.

	$\Phi_{1,1}$	$\Phi_{1,2}$	$\Phi_{2,1}$	$\Phi_{2,2}$	$\Phi_{2,3}$	$\Phi_{3,2}$	$\Phi_{3,4}$	$\Phi_{4,1}$	$\Phi_{4,3}$	$\Phi_{4,5}$
car_r0	0.1251	0.1865	0.0945	0.1672	0.0521	0.1046	0.0465	0.0255	0.0291	0.0234
car_r1	0.1332	0.1995	0.1177	0.1799	0.0617	0.1130	0.0548	0.0406	0.0344	0.0248
car_r2	0.1751	0.1473	0.1139	0.1623	0.0561	0.1127	0.0542	0.0327	0.0193	0.0090
car_r3	0.1391	0.1604	0.0771	0.1549	0.0238	0.1013	0.0500	0.0114	0.0090	0.0080
car_r4	0.1251	0.1865	0.0945	0.1672	0.0521	0.1046	0.0465	0.0255	0.0291	0.0234
car_r5	0.1438	0.1843	0.1160	0.1784	0.0550	0.1164	0.0589	0.0406	0.0289	0.0182
car_r6	0.1751	0.1473	0.1139	0.1623	0.0561	0.1127	0.0542	0.0327	0.0193	0.0090
car_r7	0.1271	0.1610	0.0690	0.1556	0.0212	0.1014	0.0498	0.0109	0.0138	0.0122
Stand. dev.	0.0209	0.0200	0.0189	0.0093	0.0156	0.0060	0.0044	0.0117	0.0088	0.0072

The scale factors from car_s1 to car_s7 are 0.2, 0.4, 0.6, 0.8, 1.3, 1.6, 2.0, respectively. The images and experimental results are shown in Fig. 2 and Table 2, respectively.

As it can be seen from Table 2, the proposed QFMM invariants remain almost unchanged under different scale transformations. Therefore, the QFMM invariants could also be a useful tool in color pattern recognition tasks that require the scale invariance.

5.3. Experiment on translation invariance

The experiment is carried out in this subsection to evaluate the effectiveness of the QFMM invariants under translation transform. A car image is shifted up, down, left and right within the image frame. The images are shown in Fig. 3. The QFMM invariants are calculated for each translation, and the results are depicted in Table 3. It can be

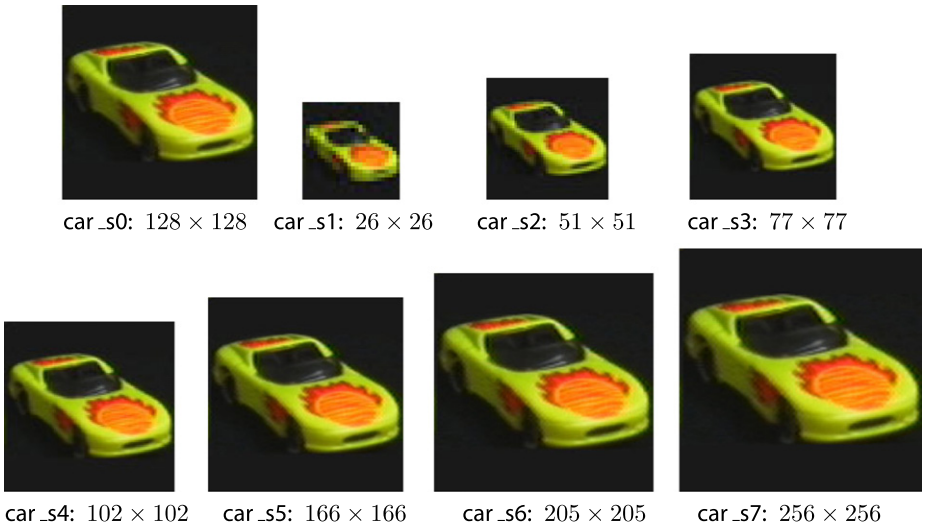

Fig. 2. The original color image and its scaled version for scale invariance tests.

Table 2
QFMM invariants of the same color image under scaling.

	$\Phi_{1,1}$	$\Phi_{1,2}$	$\Phi_{2,1}$	$\Phi_{2,2}$	$\Phi_{2,3}$	$\Phi_{3,2}$	$\Phi_{3,4}$	$\Phi_{4,1}$	$\Phi_{4,3}$	$\Phi_{4,5}$
car_s0	0.1338	0.2087	0.1238	0.2276	0.0716	0.1896	0.0882	0.0499	0.0584	0.0511
car_s1	0.1361	0.2059	0.1314	0.2282	0.0774	0.1904	0.0902	0.0628	0.0704	0.0598
car_s2	0.1342	0.2077	0.1248	0.2285	0.0727	0.1910	0.0899	0.0510	0.0602	0.0531
car_s3	0.1338	0.2083	0.1237	0.2277	0.0712	0.1897	0.0889	0.0492	0.0577	0.0505
car_s4	0.1466	0.2132	0.1627	0.2540	0.1068	0.2318	0.1297	0.1285	0.1306	0.1117
car_s5	0.1340	0.2092	0.1238	0.2275	0.0714	0.1894	0.0883	0.0493	0.0574	0.0504
car_s6	0.1343	0.2095	0.1242	0.2273	0.0717	0.1889	0.0881	0.0505	0.0585	0.0511
car_s7	0.1344	0.2097	0.1242	0.2271	0.0718	0.1886	0.0879	0.0506	0.0586	0.0511
Stand. dev.	0.0044	0.0021	0.0135	0.0093	0.0123	0.0149	0.0145	0.0274	0.0253	0.0212

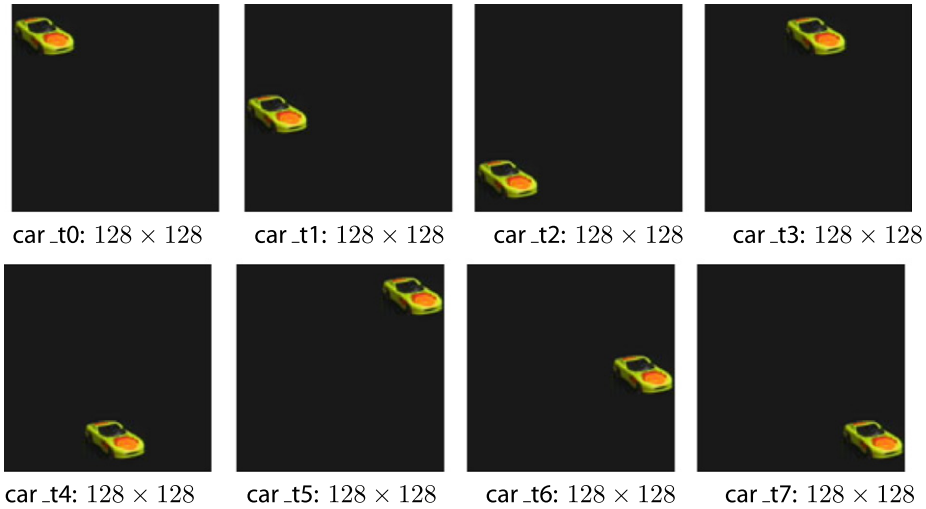

Fig. 3. The translated color image for translation invariance tests.

seen that the QFMM invariants remain almost unchanged for all translations and all the standard deviations are less than 0.02.

There is no general criterion that can be used to evaluate the stability of moment invariant. According to our experience in object recognition, if the standard deviation of the moment invariant is less than 0.1, then we can recognize the object accurately. From the bottom row of Tables 1–3, we can get the conclusions that QFMM invariants are stable under rotation, scaling and translation changes. Therefore, the QFMM invariants derived here could be useful as color image descriptors.

Table 3
QFMM invariants of the same color image under translation.

	$\Phi_{1,1}$	$\Phi_{1,2}$	$\Phi_{2,1}$	$\Phi_{2,2}$	$\Phi_{2,3}$	$\Phi_{3,2}$	$\Phi_{3,4}$	$\Phi_{4,1}$	$\Phi_{4,3}$	$\Phi_{4,5}$
car_t0	0.0562	0.0554	0.0611	0.0602	0.0587	0.0508	0.0479	0.0398	0.0383	0.0355
car_t1	0.0723	0.0701	0.0643	0.0624	0.0590	0.0434	0.0380	0.0287	0.0264	0.0220
car_t2	0.0444	0.0433	0.0609	0.0594	0.0569	0.0620	0.0556	0.0597	0.0556	0.0478
car_t3	0.0641	0.0604	0.0631	0.0592	0.0533	0.0444	0.0339	0.0321	0.0267	0.0179
car_t4	0.0664	0.0623	0.0630	0.0593	0.0533	0.0434	0.0340	0.0302	0.0260	0.0193
car_t5	0.0410	0.0398	0.0592	0.0576	0.0550	0.0632	0.0569	0.0641	0.0598	0.0522
car_t6	0.0650	0.0628	0.0633	0.0613	0.0584	0.0471	0.0427	0.0340	0.0321	0.0288
car_t7	0.0507	0.0501	0.0598	0.0591	0.0579	0.0541	0.0518	0.0458	0.0445	0.0421
Stand. dev.	0.0113	0.0104	0.0018	0.0015	0.0024	0.0080	0.0093	0.0136	0.0134	0.0133

Table 4
The right-side QFMM invariants of the same color image under rotation.

	$\Phi_{1,1}$	$\Phi_{1,2}$	$\Phi_{2,1}$	$\Phi_{2,2}$	$\Phi_{2,3}$	$\Phi_{3,2}$	$\Phi_{3,4}$	$\Phi_{4,1}$	$\Phi_{4,3}$	$\Phi_{4,5}$
car_r0	0.1161	0.1431	0.1044	0.1401	0.0624	0.0940	0.0355	0.0279	0.0309	0.0255
car_r1	0.1315	0.1499	0.1286	0.1560	0.0663	0.1043	0.0424	0.0430	0.0354	0.0264
car_r2	0.1535	0.1613	0.1150	0.1591	0.0375	0.1095	0.0542	0.0345	0.0176	0.0097
car_r3	0.1220	0.1397	0.0791	0.1400	0.0242	0.0947	0.0464	0.0131	0.0115	0.0118
car_r4	0.1161	0.1431	0.1044	0.1403	0.0624	0.0940	0.0355	0.0279	0.0309	0.0255
car_r5	0.1332	0.1617	0.1237	0.1637	0.0517	0.1102	0.0513	0.0427	0.0294	0.0209
car_r6	0.1535	0.1613	0.1150	0.1591	0.0375	0.1095	0.0542	0.0345	0.0176	0.0097
car_r7	0.1108	0.1337	0.0729	0.1367	0.0328	0.0932	0.0444	0.0122	0.0165	0.0158
Stand. dev.	0.0166	0.0111	0.0200	0.0111	0.0159	0.0079	0.0075	0.0118	0.0088	0.0073

Table 5
The right-side QFMM invariants of the same color image under scaling.

	$\Phi_{1,1}$	$\Phi_{1,2}$	$\Phi_{2,1}$	$\Phi_{2,2}$	$\Phi_{2,3}$	$\Phi_{3,2}$	$\Phi_{3,4}$	$\Phi_{4,1}$	$\Phi_{4,3}$	$\Phi_{4,5}$
car_s0	0.1286	0.1547	0.1379	0.1878	0.0835	0.1675	0.0606	0.0572	0.0668	0.0624
car_s1	0.1303	0.1528	0.1446	0.1900	0.0879	0.1706	0.0645	0.0688	0.0775	0.0705
car_s2	0.1285	0.1542	0.1392	0.1889	0.0851	0.1688	0.0615	0.0597	0.0698	0.0651
car_s3	0.1285	0.1543	0.1382	0.1877	0.0838	0.1671	0.0604	0.0578	0.0673	0.0631
car_s4	0.1397	0.1629	0.1719	0.2216	0.1103	0.2187	0.1130	0.1299	0.1325	0.1186
car_s5	0.1287	0.1553	0.1378	0.1880	0.0832	0.1678	0.0612	0.0563	0.0657	0.0617
car_s6	0.1289	0.1554	0.1382	0.1876	0.0836	0.1670	0.0607	0.0575	0.0670	0.0628
car_s7	0.1291	0.1556	0.1382	0.1875	0.0836	0.1669	0.0608	0.0575	0.0671	0.0629
Stand. dev.	0.0039	0.0031	0.0118	0.0118	0.0093	0.0180	0.0183	0.0253	0.0228	0.0195

Table 6
The right-side QFMM invariants of the same color image under translation.

	$\Phi_{1,1}$	$\Phi_{1,2}$	$\Phi_{2,1}$	$\Phi_{2,2}$	$\Phi_{2,3}$	$\Phi_{3,2}$	$\Phi_{3,4}$	$\Phi_{4,1}$	$\Phi_{4,3}$	$\Phi_{4,5}$
car_t0	0.0560	0.0550	0.0609	0.0598	0.0582	0.0505	0.0474	0.0396	0.0380	0.0350
car_t1	0.0720	0.0695	0.0639	0.0615	0.0578	0.0427	0.0365	0.0284	0.0255	0.0206
car_t2	0.0442	0.0429	0.0606	0.0588	0.0560	0.0613	0.0544	0.0593	0.0547	0.0465
car_t3	0.0643	0.0609	0.0634	0.0599	0.0542	0.0451	0.0350	0.0323	0.0274	0.0189
car_t4	0.0659	0.0614	0.0627	0.0586	0.0524	0.0430	0.0336	0.0302	0.0259	0.0193
car_t5	0.0413	0.0404	0.0597	0.0584	0.0562	0.0641	0.0586	0.0646	0.0610	0.0541
car_t6	0.0658	0.0643	0.0639	0.0625	0.0601	0.0478	0.0439	0.0341	0.0325	0.0294
car_t7	0.0507	0.0500	0.0597	0.0590	0.0578	0.0541	0.0516	0.0458	0.0445	0.0420
Stand. dev.	0.0113	0.0104	0.0018	0.0015	0.0024	0.0082	0.0095	0.0137	0.0136	0.0134

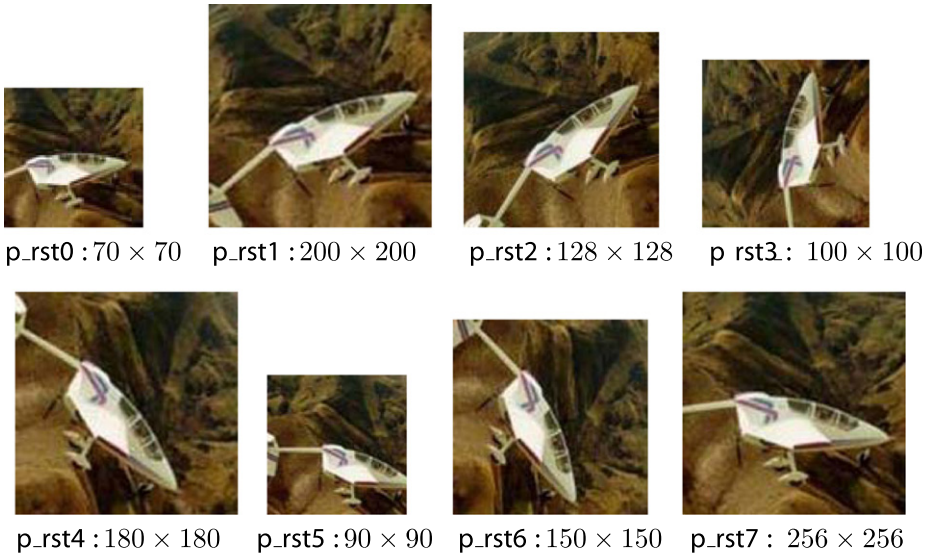

Fig. 4. The similarity transformed color images for invariance tests.

Table 7
QFMM invariants of the same color image under similarity transform.

	$\Phi_{1,1}$	$\Phi_{2,1}$	$\Phi_{2,2}$	$\Phi_{3,1}$	$\Phi_{3,2}$	$\Phi_{3,3}$	$\Phi_{4,1}$	$\Phi_{4,2}$	$\Phi_{4,3}$	$\Phi_{4,4}$
p_rst0	0.2149	0.1493	0.1743	0.1194	0.1661	0.0677	0.1099	0.1560	0.0895	0.0597
p_rst1	0.2182	0.1495	0.0924	0.1280	0.0782	0.0653	0.1260	0.0658	0.0669	0.0255
p_rst2	0.2002	0.1574	0.1200	0.1506	0.1171	0.0410	0.1550	0.1126	0.0389	0.0403
p_rst3	0.1731	0.1235	0.0424	0.1008	0.0432	0.1276	0.0964	0.0437	0.1461	0.0844
p_rst4	0.2254	0.1452	0.0787	0.1292	0.0845	0.0431	0.1349	0.0905	0.0439	0.0446
p_rst5	0.2326	0.1468	0.0244	0.1149	0.0419	0.0437	0.1057	0.0614	0.0465	0.0694
p_rst6	0.2475	0.1467	0.0526	0.1185	0.0597	0.0726	0.1162	0.0646	0.0789	0.0287
p_rst7	0.2351	0.1424	0.0938	0.1066	0.0868	0.0978	0.0985	0.0796	0.1185	0.0924
Stand. dev.	0.0232	0.0098	0.0477	0.0154	0.0412	0.0302	0.0199	0.0357	0.0382	0.0250

Table 8
Traditional FMM invariants of the same image under similarity transform.

	$\Phi_{1,1}$	$\Phi_{2,1}$	$\Phi_{2,2}$	$\Phi_{3,1}$	$\Phi_{3,2}$	$\Phi_{3,3}$	$\Phi_{4,1}$	$\Phi_{4,2}$	$\Phi_{4,3}$	$\Phi_{4,4}$
p_rst0	0.2741	0.2234	0.2030	0.1748	0.2225	0.1287	0.1421	0.2292	0.1088	0.0529
p_rst1	0.2888	0.2396	0.1411	0.1922	0.1609	0.0623	0.1635	0.1680	0.0465	0.1105
p_rst2	0.2625	0.2293	0.1338	0.1966	0.1491	0.0372	0.1778	0.1535	0.0342	0.1393
p_rst3	0.2405	0.2358	0.0742	0.2062	0.0875	0.0326	0.1880	0.0927	0.0479	0.1290
p_rst4	0.3413	0.2833	0.0739	0.2284	0.0595	0.0362	0.1888	0.0625	0.0303	0.0794
p_rst5	0.3463	0.2825	0.1055	0.2318	0.1015	0.0276	0.1972	0.0962	0.0097	0.0870
p_rst6	0.3582	0.2866	0.0429	0.2310	0.0439	0.0419	0.1938	0.0535	0.0311	0.0897
p_rst7	0.3289	0.2630	0.1243	0.2087	0.1339	0.0637	0.1713	0.1423	0.0520	0.0753
Stand. dev.	0.0441	0.0264	0.0500	0.0207	0.0586	0.0330	0.0184	0.0594	0.0291	0.0289

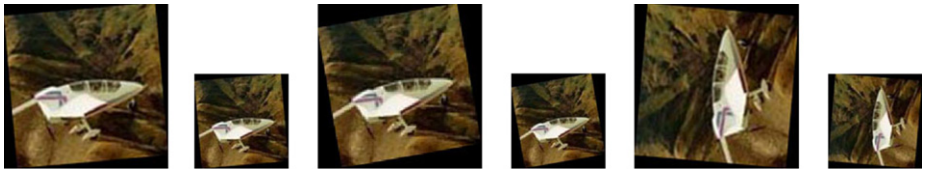

Fig. 5. The color images of simulated misalignment by rotation and scaling.

Table 9
The RMS error of rotation angle and scale factor for 34 simulations.

RMS errors	QFM-based	FFT-based
Rotation RMS	0.7227	0.7595
Scaling RMS	0.0108	0.0181

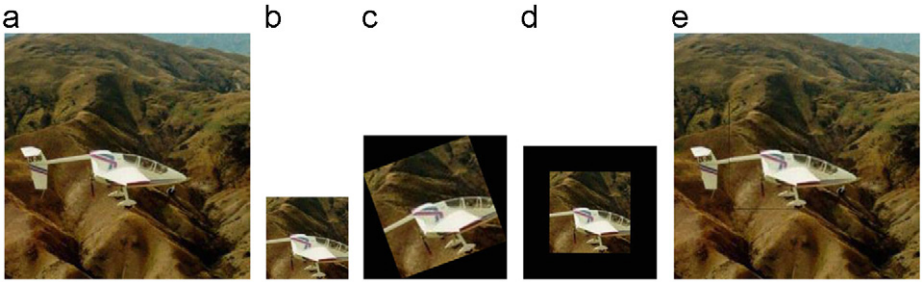

Fig. 6. The registration of color images with rotation and scaling.

5.4. Experiment on the similarity invariance using right-side QFMM invariants

In this subsection, we use right-side QFMM to construct invariants in Eq. (15), and experiment on the pictures in the last three subsections. The corresponding results are shown in Tables 4–6, respectively. As we can see from the above three tables, the right-side QFMM invariants remain almost unchanged under rotation, scaling and translation changes. Eq. (9) indicates that we can compute right-side QFMMs through left-side QFMMs, then we can get the conclusions that the left-side and right-side QFMM invariants are identical to describe the similarity transform of a color image. Therefore, the right-side QFMM invariants could also be a useful tool in color pattern recognition tasks that require rotation, scale and translation invariance.

5.5. Experiment on similarity invariance

In this subsection, we consider the situation of rotation, scaling and translation changes at the same time for real color images. The original image is downloaded from the Website [45], the similarity transformed versions are shown in Fig. 4 and the experimental results are depicted in Table 7. In order to compare the proposed technique to older methods, we change the color images to gray-level one, and compute the traditional Fourier–Mellin moment invariants. The experimental results are shown in Table 8.

Table 7 shows the QFMM invariants remain almost unchanged under different similarity transforms. Compared with Table 8, most of the QFMM invariants are stable than corresponding one. Therefore, the similarity invariants based on QFMMs perform better than those derived from traditional Fourier–Mellin moments.

5.6. Experiment on color image registration

In this subsection, we present the experimental results for registration performance of the proposed method compared with traditional FFT-based one. The efficiency of the proposed registration algorithm can be evaluated by simulating a misalignment between two color images. When the rotation and scaling parameters between two images are known, the error produced by the registration algorithm can be quantified. The original color image is 128×128 pixels, 34 simulated replicas of rotation and scaling were generated in the following way: the image is rotated from 5° to 85° and increased by 5°, then for each rotated image, we expand them by the scale factor 0.7 and 1.5, respectively. Fig. 5 shows six of these simulations. Experimental results of our method compare with FFT-based one under the measure of root-mean-squared (RMS) errors are given in Table 9. As experimental results show, the precision of the parameters estimated using our method is better than FFT-based one.

In Fig. 6, (a) is the reference image; (b) is taken from (a); (c) is scaled and rotated version of (a) with rotation angle 20° and scale factor 1.5; the estimated parameters using QFMM are: $\varphi = 20.3852$, $a = 1.5033$; (d) is recovered from (c) using estimated parameters; (e) is the result of overlying of the images (a) and (d). As it can be seen from Fig. 6, our method is suitable for registration of color image with rotation and scaling changes.

6. Conclusions

In this paper, we proposed the quaternion Fourier–Mellin moments and constructed the similarity invariants of color images. We also investigated the method of color image registration using QFMMs. The experimental results show that our method is better than traditional one which was dealing with gray-level images. In addition, the main advantage of our method is that it can process color image directly, without losing color information. Our future work will focus on the use of QFMM invariants for the application of color object recognition.

Acknowledgements

We thank the anonymous referees for their helpful comments and suggestions that improved the quality of this manuscript. Thanks are also extended to the editors for their work.

References

[1] M.K. Hu, Visual pattern recognition by moment invariants, IRE Trans. Inf. Theory 8 (1962) 179–187.
[2] Y.S. Abu-Mostafa, D. Psaltis, Recognitive aspects of moment invariants, IEEE Trans. Pattern Anal. Mach. Intell. PAMI-6 (1984) 698–706.
[3] M.R. Teague, Image analysis via the general theory of moments, J. Opt. Soc. Am. 70 (1980) 920–930.
[4] C.H. Teh, R.T. Chin, On image analysis by the methods of moments, IEEE Trans. Pattern Anal. Mach. Intell. 10 (1988) 496–513.

[5] Z.L. Ping, R.G. Wu, Y.L. Sheng, Image description with Chebyshev–Fourier moments, J. Opt. Soc. Am. A 19 (2002) 1748–1754.
[6] H.Q. Zhu, H.Z. Shu, J. Liang, L.M. Luo, J.L. Coatrienx, Image analysis by discrete orthogonal Racah moments, Signal Processing 87 (2007) 687–708.
[7] H.Q. Zhu, H.Z. Shu, J. Liang, L.M. Luo, J.L. Coatrienx, Image analysis by discrete orthogonal dual-Hahn moments, Pattern Recognition Lett. 28 (2007) 1688–1704.
[8] J. Flusser, T. Suk, Degraded image analysis: an invariant approach, IEEE Trans. Pattern Anal. Mach. Intell. 20 (1998) 590–603.
[9] J. Flusser, On the independence of rotation moment invariants, Pattern Recognition 33 (2000) 1405–1410.
[10] J. Liu, T.X. Zhang, Fast algorithm for generation of moment invariants, Pattern Recognition 37 (2004) 1745–1756.
[11] F. Ghorbel, S. Derrode, R. Mezhoud, T. Bannour, S. Dhahbi, Image reconstruction from a complete set of similarity invariants extracted from complex moments, Pattern Recognition Lett. 27 (2006) 1361–1369.
[12] A. Broumandnia, J. Shanbehzadeh, Fast Zernike wavelet moments for Farsi character recognition, Image Vision Comput. 25 (2007) 717–726.
[13] D. Xu, H. Li, Geometric moment invariants, Pattern Recognition 41 (2008) 240–249.
[14] D. Casasent, D. Psaltis, Scale invariant optical transform, Opt. Eng. 15 (1976) 258–261.
[15] T. Yatagay, K. Choji, H. Saito, Pattern classification using optical Mellin transform and circular photodiode array, Opt. Commun. 38 (1981) 162–165.
[16] Y. Sheng, H.H. Arsenault, Experiments on pattern recognition using invariant Fourier–Mellin descriptors, J. Opt. Soc. Am. A 3 (1986) 771–776.
[17] Y. Sheng, J. Duvernoy, Circular-Fourier-radial-Mellin transform descriptors for pattern recognition, J. Opt. Soc. Am. A 3 (1986) 885–888.
[18] A.E. Grace, M. Spann, A comparison between Fourier–Mellin descriptors and moment based features for invariant object recognition using neural networks, Pattern Recognition Lett. 12 (1991) 635–643.
[19] Y. Sheng, L. Shen, Orthogonal Fourier–Mellin moments for invariant pattern recognition, J. Opt. Soc. Am. A 11 (1994) 1748–1757.
[20] Q.S. Chen, M. Defrise, F. Deconinck, Symmetric phase-only matched filtering of Fourier–Mellin transforms for image registration and recognition, IEEE Trans. Pattern Anal. Mach. Intell. 16 (1994) 1156–1168.
[21] S. Derrode, F. Ghorbel, Robust and efficient Fourier–Mellin transform approximations for gray-level image reconstruction and complete invariant description, Comput. Vision Image Understanding 83 (2001) 57–78.
[22] X. Wang, B. Xiao, J.F. Ma, X.L. Bi, Scaling and rotation invariant analysis approach to object recognition based on radon and Fourier–Mellin transforms, Pattern Recognition 40 (2007) 3503–3508.
[23] H. Zhang, H.Z. Shu, P. Haigron, B.S. Li, L.M. Luo, Construction of a complete set of orthogonal Fourier–Mellin moment invariants for pattern recognition applications, Image Vision Comput. 28 (2010) 38–44.
[24] W.K. Pratt, Correlation techniques of image registration, IEEE Trans. Aerosp. Electron. Syst. 10 (1974) 353–358.
[25] R.J. Althof, M.G.J. Wind, J.T. Dobbins, A rapid and automatic image registration algorithm with subpixel accuracy, IEEE Trans. Med. Imaging 16 (1997) 308–316.
[26] A. Goshtasby, G.C. Stockman, C.V. Page, A region-based approach to digital image registration with subpixel accuracy, IEEE Trans. Geosci. Remote Sensing 24 (1986) 390–399.
[27] J.B.A. Maintz, P.A. vanden Elsen, M.A. Viergever, Comparison of edge-based and ridge-based registration of CT and MR brain images, Med. Image Anal. 1(1996) 151–161.
[28] S.H. Chang, F.H. Cheng, W.H. Su, G.Z. Wu, Fast algorithm for point pattern matching: invariant to translations, rotations and scale changes, Pattern Recognition 30 (1997) 311–320.
[29] W.H. Wang, Y.C. Chen, Image registration by control points pairing using the invariant properties of line segments, Pattern Recognition Lett. 18 (1997) 269–281.
[30] H.S. Alhichri, M. Kamel, Virtual circles: a new set of features for fast image registration, Pattern Recognition Lett. 24 (2003) 1181–1190.
[31] Q. Chen, M. Defrise, F. Deconinck, Symmetric phase-only matched filtering of Fourier–Mellin transform for image registration and recognition, IEEE Trans. Pattern Anal. Mach. Intell. 16 (1994) 1156–1168.
[32] B.S. Reddy, B.N. Chatterji, An FFT-based technique for translation, rotation and scale-invariant image registration, IEEE Trans. Image Process. 5 (1996) 1266–1271.
[33] L. Lucchese, G. Doretto, G.M. Cortelazzo, A frequency domain technique for range data registration, IEEE Trans. Pattern Anal. Mach. Intell. 24 (2002) 1468–1484.
[34] S.J. Sangwine, Fourier transforms of color images using quaternion or hypercomplex numbers, Electron. Lett. 32 (1996) 1979–1980.
[35] I.L. Kantor, A.S. Solodovnikov, Hypercomplex Number: An Elementary Introduction to Algebras, Springer-Verlag, New York, 1989.
[36] T.A. Ell, Quaternion-Fourier transforms for analysis of two-dimensional linear time-invariant partial differential systems, in: Proceedings of the 32nd IEEE Conference on Decision Control, 1993, pp. 1830–1841.
[37] T. Bulow, Hypercomplex spectral signal representations for the processing and analysis of images, Ph.D. Dissertation, Christian-Albrechts University, Kiel, Germany, 1999.
[38] S.C. Pei, J.J. Ding, J.H. Chang, Efficient implementation of quaternion Fourier transform, convolution and correlation by 2-D complex FFT, IEEE Trans. Signal Process. 49 (2001) 2783–2797.
[39] M.V. Aliev, A.M. Belov, A.V. Ershov, M.A. Chicheva, Parallel algorithms for a hypercomplex discrete Fourier transform, Pattern Recognition Image Anal. 17 (2007) 1–5.
[40] T.A. Ell, S.J. Sangwine, Hypercomplex Fourier transforms of color images, IEEE Trans. Image Process. 16 (2007) 22–35.
[41] S. Said, N.L. Bihan, S.J. Sangwine, Fast complexified quaternion Fourier transform, IEEE Trans. Signal Process. 56 (2008) 1522–1531.
[42] M.H. Yeh, Relationships among various 2-D quaternion Fourier transforms, IEEE Signal Process. Lett. 15 (2008) 669–672.
[43] S. Sangwine, N. Le Bihan, Quaternion toolbox for Matlab. Available online: 〈http://qtfm.sourceforge.net/〉.
[44] 〈http://www.cs.columbia.edu/CAVE/software/softlib/coil-100.php〉.
[45] 〈http://www.vision.caltech.edu/html-files/archive.html〉.

Liqiang Guo was born in 1982. He received the B.S. and M.S. degrees from Yanbian University Yan'Ji, China, in 2005 and 2008. He is currently pursuing the PhD degree in Changchun Institute of Optics, Fine Mechanics and Physics, Chinese Academy of Sciences. His research interests include digital signal processing and image processing.

Ming Zhu was born in 1964. He is a research fellow and Supervisor of PhD Candidates of Changchun Institute of Optics, Fine Mechanics and Physics, Chinese Academy of Sciences. His research interests include digital image processing, television tracking and automatic target recognition technology.